IEEE Access
Multidisciplinary | Rapid Review | Open Access Journal

Received 2 August 2022, accepted 7 September 2022, date of publication 12 September 2022, date of current version 19 September 2022.

Digital Object Identifier 10.1109/ACCESS.2022.3205605

RESEARCH ARTICLE

High Gain and Wideband Fabry-Perot Resonator Antenna Based on a Compact Single PRS Layer

NOUREDDINE MELOUKI[1,2], ABDESSELAM HOCINI[2], AND TAYEB A. DENIDNI[1], (Fellow, IEEE)

[1]EMT-INRS, Institut National de la Recherche Scientifique, Montreal, QC H5A 1K6, Canada
[2]Laboratoire d'Analyse des Signaux et Systèmes, Department of Electronics, University of M'sila, M'Sila 28000, Algeria

Corresponding author: Noureddine Melouki (noureddine.melouki@univ-msila.dz)

This work was supported by the Algerian Ministry of Higher Education and Scientific Research via Funding through the Projets de Recherche Formation-Universitaire (PRFU) Project under Grant A25N01UN280120180001.

ABSTRACT In this paper, a wideband and high gain Fabry Perot Resonator Antenna (FPRA) is proposed. It is based on a synthesized compact single partially reflective surface (PRS) layer acting as a superstrate to a slot-coupled feed antenna, which acts as a radiating source element for the proposed design. The PRS is based on a 2-D printed unit cell, where the lower part is a simple circular ring Frequency Selective Surface (FSS), incorporated with a synthesized FSS unit cell, using an automated system through a VBA based interface established between CST Microwave studio and Matlab, and optimized using a binary genetic algorithm. This new FSS layer acts as the upper part of the proposed PRS layer and provided a positive phase gradient. It almost perfectly resembles that of the optimum PRS over the desired frequency range, with a relatively high reflection magnitude, which makes it a promising superstrate candidate for wideband and high gain FP resonator antennas. The fabricated prototype achieved an important performance in terms of impedance bandwidth with 42%, ranging from 11.32 to 17.35 GHz. In addition, the 3-dB gain bandwidth is 36 % from 11.68 to 16.78 GHz, with a maximum peak gain of 14.72 dB achieved at 16 GHz. Consistent and almost invariant radiation patterns are achieved over the Ku-band frequency band of interest. The experimental and simulated results are in good agreement, justifying the feasibility of the proposed design as a high gain and wideband FP resonator antenna.

INDEX TERMS Ku-band, compact, partially reflective surface (PRS), fabry perot resonator antenna (FPRA), frequency selective surface (FSS), genetic algorithm (GA), high-gain, wideband.

I. INTRODUCTION

With the increasing demand for high-data rates and low latency wireless communication systems, wideband and highly directive antennas are becoming attractive subjects in both the academic and industrial sectors, especially in the upper microwave region and the untapped millimeter wave spectrum [1]. High gain antennas have been designed using traditional technologies such as reflectors, waveguide horn antennas [2], [3], and microstrip fed patch arrays [4]; however, these aforementioned techniques have some major disadvantages in terms of design complexity, high fabrication cost, and feeding-network induced losses.

The associate editor coordinating the review of this manuscript and approving it for publication was Qi Luo.

A Metasurface, on the other hand, is a two-dimensional equivalent of a metamaterial that is essentially a surface distribution of electrically small scatterers capable of manipulating and controlling electromagnetic waves. References [5], [6], can offer novel properties such as ultra-low profile and improved performance in gain, radiation pattern, and bandwidth. These Metasurfaces have many other inherent advantages, including their use in wave polarization controlling capabilities, for instance the conversion from linear to circular polarization [7], [8], and Multifunctional Coding Metasurfaces, like in the case of [9], which achieves Multiple Beams functionality for both left and right CP, by using Metasurfaces.

Another approach to tackle the aforementioned disadvantages, is by using a Fabry-Perot Resonator Antenna

(FPRA), [10] which consist of a partially reflective surface (PRS) based superstrate placed at a distance (usually half a wavelength) from the ground plane, creating an air-gaped cavity, and excited by a feeding source antenna (single or array) backed by the ground-plane, making this type of technique a simple, and cost effective approach for achieving a significant enhancement, as in the case of [11], where the printed ridge-gap waveguide technology is incorporated with a Fabry-Perot cavity. In addition, by using a positive phase gradient dual-layer PRS operating at 60 GHz, the proposed antenna achieved 18.4% impedance bandwidth, ranging from 55.4 to 66.6 GHz, and a 12.5 % 3 dB gain bandwidth, from 58.6 to 66.4 GHz. Moreover, the maximum peak gain is 16.8 dB, which is 12.2 dB more than the reported feed antenna gain, proving the feasibility of using such approach in terms of enhancing the antenna radiation characteristics [12], [13], [14], [15].

However, this kind of antenna suffer even more from the inherent narrow bandwidth due to the fact that the antenna's characteristics, such as its frequency, radiation patterns, gain and bandwidth are mainly determined by the PRS layer properties, and this latter invokes the typical narrow band cavity [16].

To overcome this issue, many studies have been conducted to improve the operation bandwidth while keeping higher gain performance of the FPRA. In [17] and [18], a multi-layer superstrates based on periodically printed FSS arrays have been used for bandwidth enhancement on a single and dual-band application, whereas in [19] a dielectric based one has been used to achieve a broadband EBG resonator. A side of improving the bandwidth, using multi-layer superstrates increases the profile of the antenna making it a bulky structure.

Another effective technique yet a complicated one, which involves making a dielectric slab with gradient permittivity as in [20] and [21].

A more convenient method using double-sided printed metallic layers on a dielectric medium, has attracted the interest of many researchers [22], [23], [24], since this superstrate produces a positive reflection phase gradient over a particular range of frequencies to broaden the 3-dB gain bandwidth of the FP resonator antenna, while keeping a degree of compactness and low profile, since the height of the resonance cavity is only a half wavelength. This design not only provides a high gain but also low fabrication cost.

Therefore, the main objective of this study is to design a wideband, compact, and low-profile FPRA with high gain.

In this work, a compact PRS based layer is proposed as a superstrate to an aperture-coupled wideband source antenna, to form a Fabry-Perot Resonator and to improve its gain bandwidth. The proposed PRS unit cell is generated using an automated topology synthesizing system, established using a link between the genetic algorithm embedded in Matlab and the commercial simulator CST Microwave Studio through a VBA based connection. A binary particle swarm optimization (BPSO) algorithm [25] can also be used instead of the genetic algorithm to achieve the same objective of a compact with positive reflection phase gradient PRS unit cell.

The proposed PRS design's main distinguishing features are its compactness and small footprint in comparison to dielectric-based designs, which have a complicated fabrication process (dielectric slab with gradient permittivity) [20], [21], and a larger foot print. It is low in profile, easy-to-fabricate, and cost-effective design. In addition, using 3D printing techniques could reduce fabrication costs, in combination with the proposed synthesizing system, and could achieve a compact, low profile, yet effective design. However, current 3D printing processes are far from achieving the same performances as the PCB printing techniques using small footprint structure as the one proposed here, and not yet explored to the extent where it could replace it. For example, in [26], a 3-D printed FPRA, was designed with a paraboloid-shape superstrate for wider gain bandwidth in comparison with the commonly adopted planar superstrate, and achieved 22.2% gain bandwidth with a footprint of 4 λ_0 x 4 λ_0 x 0.66 λ_0(λ_0 at 6GHz), in comparison to the proposed design with a footprint of only 1.72 λ_0 x 1.96 λ_0 x 0.62 λ_0 and 3-dB gain bandwidth of 36%.

The simulation results yield an important improvement in terms of impedance and 3-dB gain bandwidth, while keeping the compactness of the final design footprint. The proposed prototype was fabricated, and the results were verified experimentally, and they are in good agreement with the full-wave simulation results. With these features, this antenna can be a protentional candidate for the Ku-band applications with higher gain and wideband requirements.

The proposed FPRA antenna as per our knowledge, is the first of its kind in the literature that uses such Partially Reflective Surface, that has been artificially synthesized, in a way where it's reflection phase response, resembles that of the optimum phase, which satisfies the cavity resonance condition according to the ray-tracing analysis, to operate in wider frequency band with relatively high gain.

The proposed designing process also, allows easy frequency tuning, using the proposed AI driven synthesizing system. Hence, this antenna can be easily scaled to different frequencies, which makes the operation more flexible.

II. PROPOSED WIDE BAND FPRA ANTENNA

Fabry-Perot resonator antenna (FPRA) is considered a highly directive one [27]. It consists of a simple radiating source backed by a ground-plane, and a partially reflecting surface (PRS) (see Fig. 1).

Gain and directivity improvements are achieved, when the spacing h_c between the ground and the PRS, satisfies the cavity resonance condition according to the ray-tracing analysis, where the reflected waves from the ground and the reflection phase response of the PRS are in phase, leading to the maximum peak gain in the broadside direction [28], and the spacing h_c equals to the following:

$$h_c = \frac{c}{4\pi f_r}\left(\varphi_{PRS} + \varphi_{GND} - 2N\pi\right) \tag{1}$$

where φ_{PRS} and φ_{GND} are both the reflection phases of the PRS and the ground plane, respectively. N is the resonance mode order, and is equal to 0,1, 2,...etc. For a low profile Fabry-Perrot based resonator antenna, N is set to be 0. f_r and c are the resonance frequency and the speed of light in the vacuum, respectively.

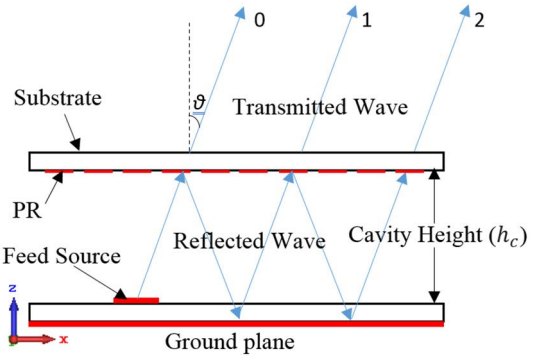

FIGURE 1. Schematic diagram of a Fabry-Perot resonator.

Assuming that the source antenna directivity is D_{ref} at a particular frequency f_r, the directivity of the FPRA antenna would be the summation of this latter and the PRS directivity D_{PRS}, which is expressed as:

$$D_{PRS} = 10\log\left(\frac{1+\Gamma}{1-\Gamma}\right) \tag{2}$$

where Γ is the reflection magnitude of the PRS superstrate layer, and the total theoretical FPRA directivity is formulated as follows [1]:

$$D_{FPRA} = D_{ref} + D_{PRS} \tag{3}$$

From Equations (2) and (3), it is clearly noticed that the directivity of FPRA is positively correlated with the PRS reflection amplitude, thus, the larger this latter is, the better the overall directivity of the FP resonator antenna.

Due to the fact that the cavity spacing h_c and the partially reflective surface phase φ_{PRS}, are frequency-sensitive, conventional FPRAs only possess a small radiation bandwidth.

Assuming that the dielectric slab is lossless, the aperture surface of the FPRA for a required directivity can be approximated using the following formula [29]:

$$A = \frac{10^{\frac{D_{FPRA}}{10}}\lambda^2}{\pi^2} \tag{4}$$

where λ is the operating wavelength of the FPRA.

By taking a PEC ground plane ($\varphi_{GND} = \pi$), the PRS reflection phase is expressed by rearranging (1) as the following:

$$\varphi_{PRS} = \frac{4\pi h_c}{c} f_r + (2N-1)\pi \tag{5}$$

From (5) it can be noted that if the reflection phase of the PRS increases with the resonance frequency f_r (a positive slope versus frequency), the FPRAs would operate in a wider frequency band with an enhanced gain bandwidth. Therefore, a PRS with positive reflection phase gradient is needed, for designing a wideband and high gain Fabry Perrot based Resonator Antenna. To elaborate on this, let us consider that the superstrate dielectric slab is lossless, with the reflection magnitude is equal to 1, and we only consider the phase of the reflection coefficient (φ_{PRS}), which is formulated as [30]:

$$\varphi_{PRS} = \pi - 2\arctan(Z_d \tan(k_d h_{PRS})/Z_0) \tag{6}$$

where, Z_d and Z_0 are the characteristics impedances of the dielectric substrate and the air, respectively, k_d is the dielectric phase constant, with a thickness of h_{PRS}.

When the dielectric substrate uses Rogers RT/duroid 5880 dielectric slab ($\varepsilon_{r1} = 2.2$, $\tan\delta = 0.0009$), with a thickness h_{PRS} of 1.575 mm, and according to (6), its reflection coefficient phase response is depicted in Fig. 2, Where it is clearly seen that the phase of the reflection coefficient decreases as the frequency increases, when the height is kept constant. Consequently, if the PRS shows positive phase gradient as per (6) and from the results in Fig. 2, the FPRA is able to operate in a wideband of frequencies. Moreover, since the ground plane of the FPRA is a PEC($\boldsymbol{\varphi_{GND}} = \pi$), the Fabry-Perot antenna can operate in wide frequency band when the PRS exhibits even smaller positive reflection phase response, and not necessary covers the whole band of interest.

A. PROPOSED PRS STRUCTURE

In the previous section, a PRS with a positive phase gradient is discussed to be the main key point for designing a wideband FP resonator antenna. Therefore, first of all, we should carefully design one that meets the aforementioned requirement.

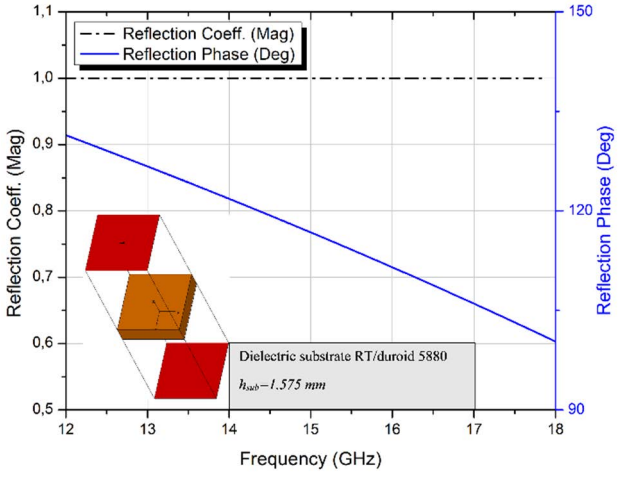

FIGURE 2. Reflection phase and magnitude of substrate versus incident wave frequency.

First, a simple circular ring is etched on one side of a Rogers RT/duroid 5880 dielectric slab ($\varepsilon_{r1} = 2.2$, $\tan\delta = 0.0009$), with a thickness h_{PRS} of 1.575 mm, creating the initial PRS unit cell having the following design parameters:

w_{PRS}=*6* mm, r_o=*2.9* mm, r_i=*1.4* mm and $g = 0.2$ mm. Fig. 3(a) shows the geometry of the initial PRS unit cell.

The PRS unit cell is designed and simulated using CST Microwave studio, and the reflection phase characteristics analyzing setup is depicted in Fig. 3(b), where boundary conditions are applied as follow: along the ± x-axis, the perfect magnetic condition (PMC) is applied, whereas, in the case of the ±y-axis, the perfect electric boundary condition (PEC) is used, with two wave ports set at a distance of $\lambda/2$ from the unit cell under investigation along the z-axis, with open boundary condition, so only the normal incidence is considered here.

The simulated magnitude and phase of the reflection coefficient response of the initial PRS unit cell are shown in Fig. 4. Where it's noticed that the PRS unit cell is highly reflective around the frequency band of interest with a magnitude of $\Gamma = 0.9$ at 15 GHz. A high reflection magnitude is targeted for a high gain antenna. However, the reflection phase of the unit cell as depicted in Fig. 4, is decreasing as the frequency increases, which leads to a narrower bandwidth. A new unit cell that provides a positive reflection phase gradient is then proposed to broaden the antenna bandwidth while keeping a high gain performance.

A partially reflective surface (PRS) unit cells are printed on either one or both sides of the dielectric slab, just like in this case, where it is printed on both sides of the same dielectric substrate used on the previous PRS design, namely the Rogers RT/duroid 5880, with the same thickness of 1.57 mm.

The next approach is based on the same PRS unit cell, and uses a pixelated based pattern on the other side of the unit cell, to create a positive phase gradient that follows the optimal phase, for increasing the bandwidth.

Genetic algorithm (GA) based optimizations were carried out, yielding great potential in finding non-conventional solutions to EM-based problems.

In [31], the genetic algorithm has been used to optimize an EBG structure for gain and bandwidth enhancement, whereas in the case of [32], an AMC based reflector has been optimized using the same technique to achieve an important enhancement in the peak gain and front-to-back ratio, alongside a low side-lobe level (SLL), for 5G applications. On the other hand, to improve the gain of an UWB monopole antenna, in [33] a compact UWB FSS structure was created using a similar GA based synthesizing system, with specific parameters in terms of the targeted structure and the fitness function, totally different than the current work objectives, where the FSS unit cell was divided into square pixel cells, represented by binary bits of 1 and 0.

Throughout the optimization process, each binary word generated by the GA corresponds to a potential solution that is analyzed and evaluated, using a predefined fitness function. This latter is defined as the sum of all values that exceed −10 dB of the unit cell transmission coefficient (S_{21}), in order to achieve a broad band-stop performance between 3.1 and 10.6 GHz (UWB spectrum), forming an FSS-based reflector for gain enhancement. Since different fitness and objective functions are used in various electromagnetic-related problems implemented in various applications, this reported work is only somewhat relevant to the current one in terms of using the GA-based optimization process.

The well-established VBA-based connection between CST Microwave studio and MATLAB's embedded genetic algorithm (GA) is used here, to create the automated pattern synthesizing system, where the upper side of the PRS structure is the targeted area for this procedure. Each PRS unit cell is pixelated into n x m pixels, and these latter are defined using binary encoding, where having the value of either 1 or 0 indicates the presence or the absence of copper on the pixelated sub-cell (on top of the dielectric slab).

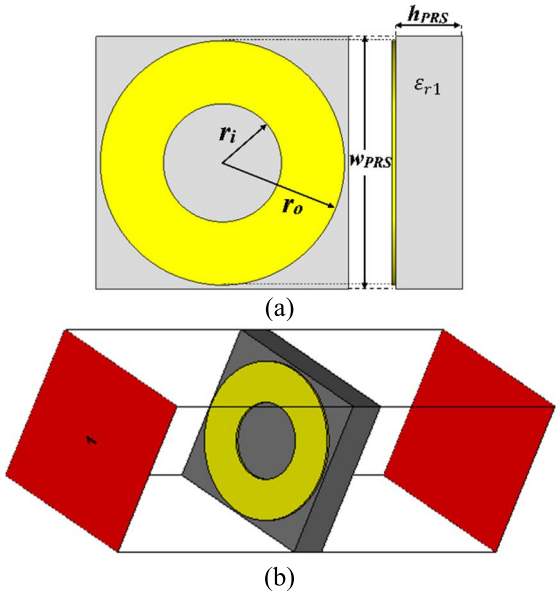

FIGURE 3. (a) Geometry of the initial PRS unit cell, (b) Analysis setup of the unit cell (CST).

Increasing the number of pixelated cells, increases also the number of total possible structures, making it an impractical way in solving such a problem, so, a confined search space global optimization solution is needed, for finding the optimal candidate, according to a predefined fitness function, making the genetic algorithm an effective way in doing so.

In the proposed designing scenario, the fitness function is defined as the root-mean-square error (RMSE) between the reflection coefficient phase response of the generated PRS unit cell under investigation, and the optimum phase, and is defined as:

$$\text{Fit} = RMSE(Phase_{PRS}, Phase_{Optimum}) \tag{7}$$

where RMSE is defined as:

$$RMSE = \sqrt{\frac{\sum_{n=1}^{N} \left(Phase_{PRS} - Phase_{Optimum}\right)}{N}} \tag{8}$$

The reflection coefficient phase of the PRS unit cell is taken at equal frequencies fi, with the total number

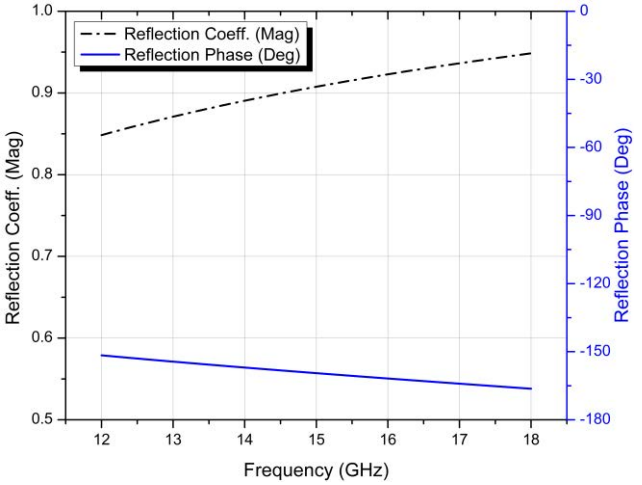

FIGURE 4. Reflection phase and magnitude of the initial PRS unit cell.

of N = 1001 frequency points, within the designated overlapping frequency band of interest ($f_{min} \leq fi \leq f_{max}$).

The implemented flowchart of the GA-based optimization process for a positive phase gradient PRS unit cell is shown in Fig. 5. As a starting point, the PRS unit cell is discretized into 12 × 12 pixels, which provides a resolution of 0.5 × 0.5 mm, which is chosen while taking into account the fabrication constraints and maintaining the geometrical flexibility.

A 12 x 12 discretized unit cell needs to be represented by 144 binary encoded pixels, and this led to large search space for the optimal solution, which is an impractical and time-consuming process. To overcome this, a four-folded symmetry is imposed, as shown in Fig. 6. As a result, the search space for the optimal solution (the number of bits required to represent the PRS unit cell) is reduced drastically to 21.

The proposed optimization process tries to manipulate the reflection coefficient phase of the possible PRS design candidates, to produce a PRS unit cell with a phase that closely resembles the positive gradient optimum phase, within the frequency band of interest, by using the proposed genetic algorithm, with a uniform mutation at a rate of 0.001, a single point crossover, and the tournament selection as its parameters.

The population size is set to be 200 different binary strings randomly selected, with each one representing a specific pixelated PRS unit cell, and the number of iterations (generations) is set to be 20.

Once all the 200-initial pixelated PRS structures are evaluated, they are ranked and the top-performing ones are selected for the crossover and mutation processes, creating a new population of 200 PRS candidates going through the same evaluation process. This later is repeated until the desired fitness value is achieved (*Fit* tends toward zero) or until the maximum number of iterations is reached.

The best achieved PRS design is obtained at the 10th iteration, when the stop criterion is met, as shown in Fig. 7.

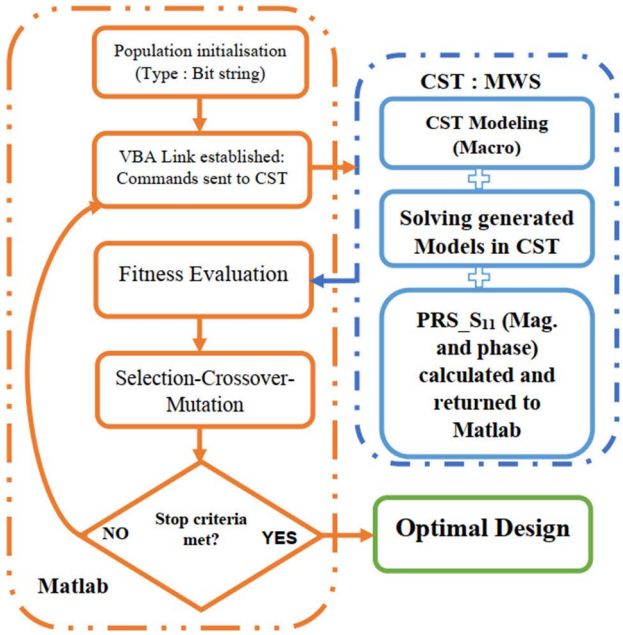

FIGURE 5. Proposed flowchart of the GA optimization process for the PRS unit cell.

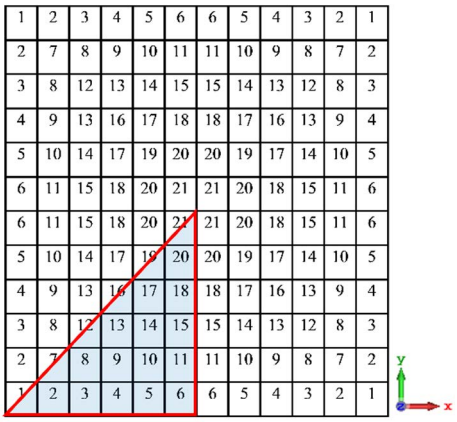

FIGURE 6. Proposed four-folded symmetry pixelated PRS unit cell (12×12).

a, where it is clearly shown that the final design doesn't suffer from the infinitesimal connection problem, between two sub-cells, when these constellations $\binom{10}{01}$ or $\binom{01}{10}$ are present, which could lead to a malfunctioning PRS structure, due to fabrication tolerances. Also, since the design imposes the four-folded symmetry, the PRS unit cell exhibits polarization insensitivity, which makes it also applicable to circular polarized antennas.

The binary string of the final optimized PRS unit cell is: $B_{PRS} = \{0\,1\,0\,1\,0\,0\,1\,1\,1\,0\,1\,0\,0\,0\,1\,1\,1\,1\,1\,0\,0\}$.

The resulted reflection coefficient phase of the optimized PRS has a positive gradient and is almost perfectly resembles that of the optimum PRS over a wide bandwidth spectrum range, with a relatively high reflection magnitude (See Fig. 7. b), and this can be a vital key point in designing a

wideband with high gain FPRA antenna, since higher reflective PRS leads to higher gain as per (2) & (3) but narrower −3 dB bandwidth, and to broaden this latter a PRS with positive phase gradient is a must to achieve that goal, as per (5). So a compromise between the maximum achieved gain and the −3 dB gain bandwidth, is inevitable, and this can be seen in the following sections. Nerveless, the proposed PRS design can be a potential superstrate candidate for a wideband and high gain FP resonator antenna.

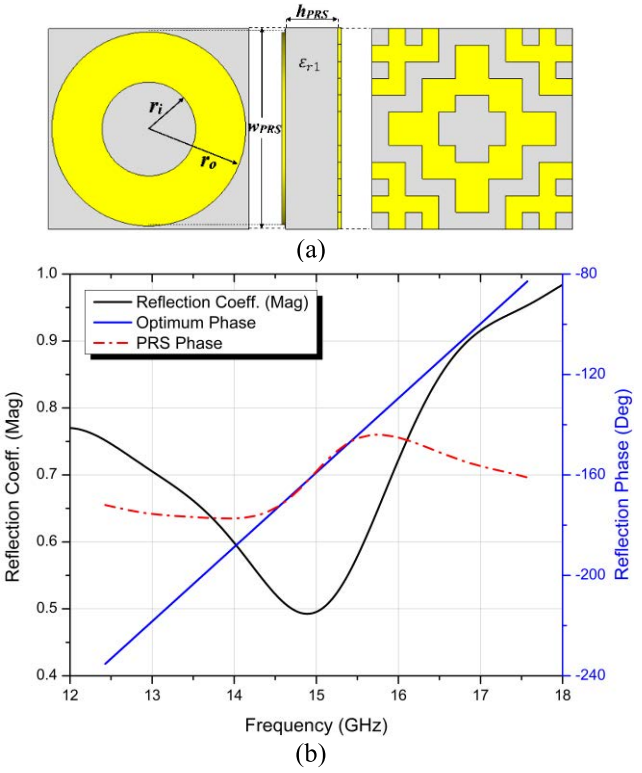

FIGURE 7. (a) GA based final optimized PRS design, and (b) reflection coefficient's magnitude and phase of the proposed PRS unit cell.

B. FEEDING ANTENNA

The feeding source antenna for an FPRA is as vital to its performance as the PRS structure, thus a well-designed feeding antenna is a crucial part of designing a high gain and wideband FPRA antenna. Several types of exciting sources have been reported in the literature, such as a suspended metal strip over a ground plane [16], a probe-fed patch antenna [34], and a waveguide aperture-based feeding [35]. Single layer slot-coupled antenna can be also used, as feeding element, like in the case of [36], where the feeding antenna was an isosceles triangular-shaped slot-coupled, to a 50-Ω feed line printed on the bottom face of the same ground-backed substrate.

An air-gapped slot-coupled patch antenna is a good candidate for a high gain and wideband FPRA antenna, due to its low profile, ease of feeding and fabrication, stable broadside radiation, and wide bandwidth capability.

The proposed feed antenna design is depicted in Fig. 8. it consists of a parasitic patch, coupled to a feeding line through a slotted ground plane (bottom layer), and spaced by an airgap $h_{air} = 2$ mm, for surface waves suppression since this latter can contribute to performance degradation of the FRPA cavity [37]. An impedance matching network is added to the feedline to improve the bandwidth. The Rogers RT/duroid 5880 material having a thickness (h_s) of 0.787 mm, permittivity $\varepsilon_{r2} = 2.2$, and a loss tangent of 0.0009, is used as a substrate for both the parasitic patch and the bottom layer (ground plane and the feed line). The antenna design parameters are summarized in Table 1.

Both the simulated reflection coefficient (S_{11}) and the peak gain of the feed antenna are illustrated in Fig. 9. a, where it is noticed that the impedance bandwidth almost covers the whole Ku-band spectrum, ranging from 12.6 GHz to 18 GHz. Within this band, the peak gain increased from 7 to 8.8 dBi. In addition, the co- and cross-polarization patterns at 16 GHz, in both the E-and H-planes are illustrated also in Fig. 9. b & c. respectively, with low cross-polarization in both cuts, making it a good candidate for being a feeding source for the proposed FRPA antenna to be designed in the next section.

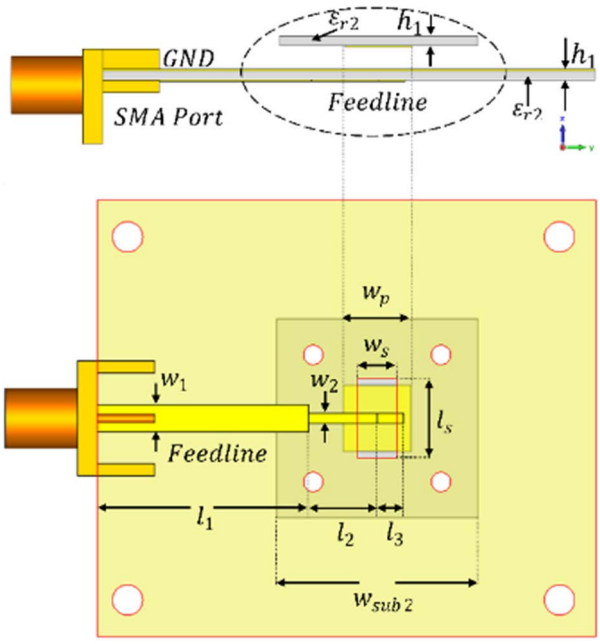

FIGURE 8. Schematic diagram of the slot-coupled patch antenna.

C. PROPOSED FPRA ANTENNA

The optimized PRS structure (Fig. 7) is applied as a superstrate layer to the proposed slot-coupled feed antenna in the previous section (Fig.8), creating the proposed wideband and high gain FP resonator antenna as shown in Fig. 10.

The PRS superstrate is suspended over the shared ground plane at a distance h_c using M2 nylon screws (2 mm in diameter) at the four corners, and they are also taken into account during the simulation process, alongside a 50 Ohm

TABLE 1. Slot-coupled patch antenna design parameters.

Ant. Parameter	h_1	w_1	w_2	l_1	l_2
Value (mm)	0.79	2.3	0.9	17.4	5.6
Ant. Parameter	l_3	w_s	l_s	w_p	w_{sub2}
Value (mm)	2.2	3.2	6.5	5.5	16.5

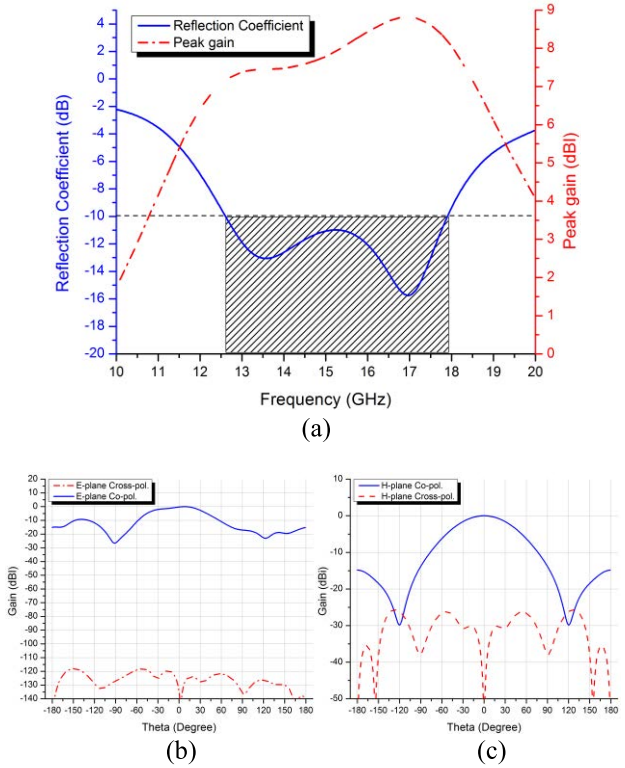

FIGURE 9. Simulated results of the slot-coupled patch antenna (a) reflection coefficient, peak gain, and (b & c) the normalized E- and H-plane radiation patterns 16 GHz, respectively.

SMA connector modeled also in CST Microwave studio. A preliminary determination of h_c can be achieved using both the simulated results of the proposed PRS unit cell reflection coefficient phase (φ_{PRS}) in Fig. 7 (b) and (1), where f_r is the FPRA's center frequency and φ_{PRS} is taken also at that same center frequency.

The reflection coefficient phase of the PRS at the center frequency of 15GHz is about $-158.6°$ (see Fig. 7(b)), and by using (1), the spacing h_c is about 10.5mm. Further optimization is need to be performed to find the optimal distance to achieve the best performance of the Fabry-Perot Resonator Antenna.

The aperture size of the proposed FPRA antenna is estimated by using (4), where the wavelength λ is taken at the lower end frequency (12.6 GHz) of the antenna, which is 23.8 mm, and the corresponding estimated FPRA directivity (D_{FPRA}) is around 13.73 dBi using both (2) and (3), therefore, the aperture size is about 36.83 mm x 36.83 mm.

Thus, a PRS structure of an aperture size of 36mm×36mm is used as the superstrate for the proposed FP resonator antenna, which consists of an array of 6 × 6 PRS unit cells since this latter's effective size is 6 mm.

Using the previously estimated parameters, namely the aperture size (36mm x 36mm), and the cavity air gap h_c = 10.5 mm, the resulted reflection coefficient S_{11} of the proposed FPRA is illustrated in Fig. 11, where the impedance bandwidth ($|S11| < -10$dB) is about 3.24 GHz divided into a dual-band, ranging from 14.18 to 16.52 GHz, and from 17.1 to 18 GHz. The peak gain is 14.4 dBi at 14.5 GHz.

The air gaped cavity of the FP resonator antenna is an important factor in designing a wideband antenna with high gain; therefore, the influence of changing such a parameter on the overall performance of the proposed antenna is investigated.

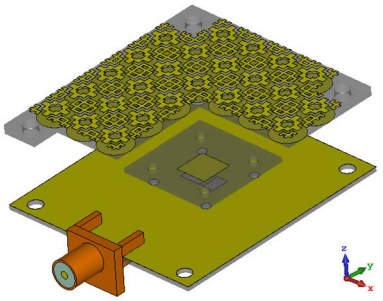

FIGURE 10. Proposed wideband FPRA design.

All other parameters are fixed, while the cavity height is changed in a step of 0.5 mm from 10.5 to 13 mm, to see the effect of the cavity height variation on the S_{11} impedance bandwidth, the peak gain, and the 3-dB gain bandwidth of the FPRA. The results are depicted in Fig. 11 & 12 and summarized in Table 2. From there, it is noticed that when the cavity thickness increases, both the impedance and 3-dB gain bandwidths are gradually expanded, while the peak gain is reduced, accordingly, as expected from an FP resonator antenna.

For a high gain FP resonator antenna with a wider operating bandwidth, and based on the results illustrated in both Fig. 11 & 12, and Table 2, it can be concluded that the optimal cavity height is 13 mm, where the proposed FPRA exhibited an outstanding impedance bandwidth performance of 38.64% ranging from 11.9 to 17.6 GHz (Fig. 11), and a 3-dB gain bandwidth of 39.11% (11.6 to 17.24 GHz), with a maximum peak gain of 14.21 dBi at 16 GHz as shown in Fig. 12.

Another important parameter that considerably influences the FPRA peak gain and bandwidth is its PRS superstrate size, therefore, the influence of changing such a parameter on the performance of the proposed antenna is investigated.

All other parameters are kept fixed, while the size of the superstrate is changed by increasing the number of PRS unit

TABLE 2. Summarized results of the proposed design at different cavity spacings.

Cavity spacing h_c (mm)	|S11|<-10dB BW (GHz)	3-dB gain bandwidth (GHz)
10.5	14.18-16.52 (15.24 %) 17.1-18 (5.12 %)	13.3-17.8 (28.93%)
11	13.29-15.2 (13.40 %) 15.71-17.68 (11.79 %)	13-17.6 (30.06%)
11.5	12.95-17.56 (30.21 %)	12.77-17.38 (30.58%)
12	12.61-17.51 (32.53 %)	12.4-17.3 (32.99 %)
12.5	12.26-17.52 (35.32 %)	11.99-17.26 (36.03 %)
13	11.9-17.6 (38.64 %)	11.6-17.24 (39.11 %)

cells, to see the effect of this variation on the peak gain, and the 3-dB gain bandwidth of the FPRA. The results are depicted in Fig. 13. From there, it is noticed that, when the superstrate size increases, the 3-dB gain bandwidth is gradually decreased, while the peak gain is increased, accordingly, achieving a maximum value of 16.67 dBi, as expected from an FP resonator antenna.

The best-achieved performance in terms of peak and gain bandwidth is when a 6 × 6 PRS superstrate is used.

Radiation patterns at three different frequencies (12.5, 14, and 16 GHz) in both E-and H- planes are simulated and depicted in Fig. 16. From this figure, it can be noted that the patterns are directive, with narrower beamwidths, because the beamwidth decreases with increasing size and frequency, meaning the beamwidth is proportional to the ratio wavelength to the antenna dimension, Thus, higher frequencies have a smaller wavelength; and since the size of the antenna is fixed, higher frequencies have a narrower beamwidth, high gain and are more directional, and according to the directivity equation [38]:

$$D = \frac{4\pi.U}{P_{rad}} \tag{9}$$

where U is the radiation intensity in watts per unit solid angle, and P_{rad} is the total radiated power in watts; at higher frequencies, the radiated power is low, meaning the directivity is high, and therefore the beamwidth is narrower, and are inversely proportional to each other. For example, the beamwidth decreased as the frequency increased from 12.5 to 16 GHz, where it was 30.1° and 33.6° at 12.5 GHz and got narrower to the values of 20.4° and 26.4° in the E- and H-planes respectively, at 16 GHz.

III. FABRICATION & MEASUREMENTS RESULTS

In this section, the prototype validation process is carried out, by first fabricating all parts involved in the proposed design with its final optimized dimensions on the Roger RTduroid 5880 dielectric slab with two different thicknesses for both the feed antenna (0.787 mm) and the proposed PRS based superstrate (1.57 mm). They are assembled using nylon M2& M3 metric pan head screws with the proper washers and hex nuts, to form the final proposed prototype (see Fig. 14(a)).

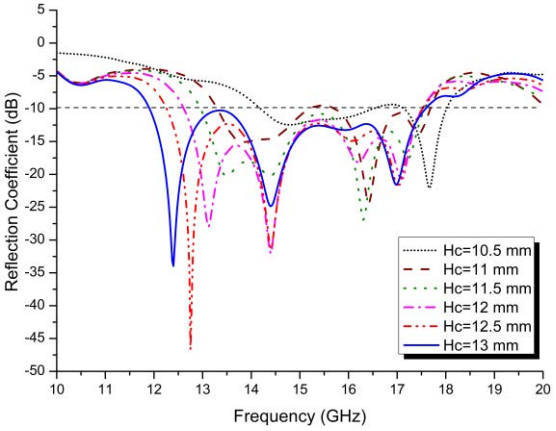

FIGURE 11. Simulated reflection coefficient of the proposed FPRA at different h_c.

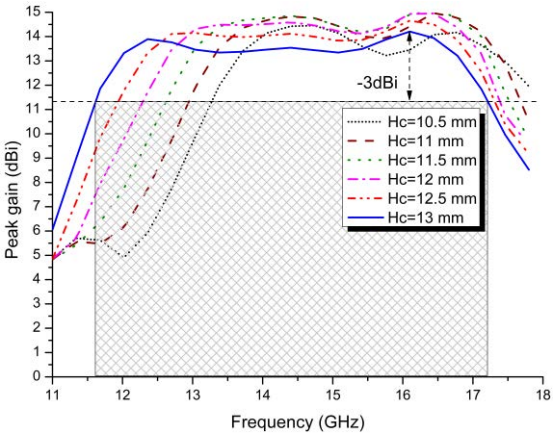

FIGURE 12. Simulated peak gain of the proposed FPRA at different values of h_c.

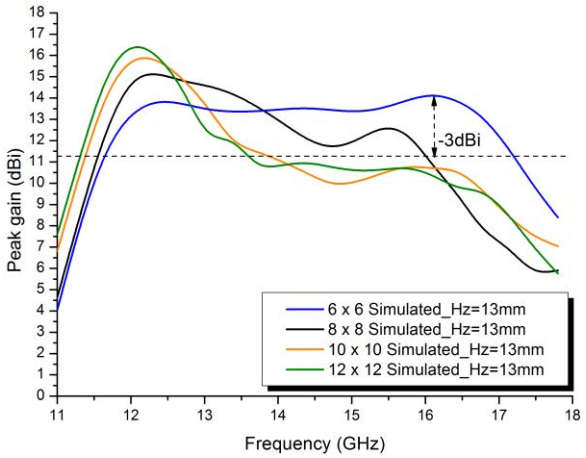

FIGURE 13. Simulated peak gain of the proposed FPRA for different PRS based superstrate sizes.

The optimal cavity spacing is fixed to 13 mm for further results validation and analysis. It is fed by a 50 Ohm SMA connector soldered to the feed line with an offset of 5 mm from the edge of the feed antenna.

TABLE 3. Proposed FPRA design compared to other related works.

Ref. No	|S11|<-10dB BW (%)	3-dB gain bandwidth (%)	Antenna electrical dimensions (W x L x H)	Max gain (dBi)	Num. of PRS layers
[1]	25.1	33.5	2.23 λ_0 x 2.23 λ_0 x 0.54 λ_0	13.92	1
[12]	26.26	28	2.4 λ_0 x 2.4 λ_0 x 0.55 λ_0	13.8	1
[33]	127.05	53.65	2.2 λ_0 x 2.2 λ_0 x 0.62 λ_0	9.7	1 (FSS)
[40]	10.90	10.9	3.67 λ_0 x 3.67 λ_0 x 0.75 λ_0	15	3
[41]	30	25.8	2.40 λ_0 x 2.40 λ_0 x 1.40 λ_0	15	2
[42]	15.06	15	3.90 λ_0 x 3.90 λ_0 x 1.70 λ_0	20	3
[43]	27	27	2.36 λ_0 x 2.36 λ_0 x 1.23 λ_0	14	2
This Work	42	36	1.72 λ_0 x 1.96 λ_0 x 0.62 λ_0	14.72	1

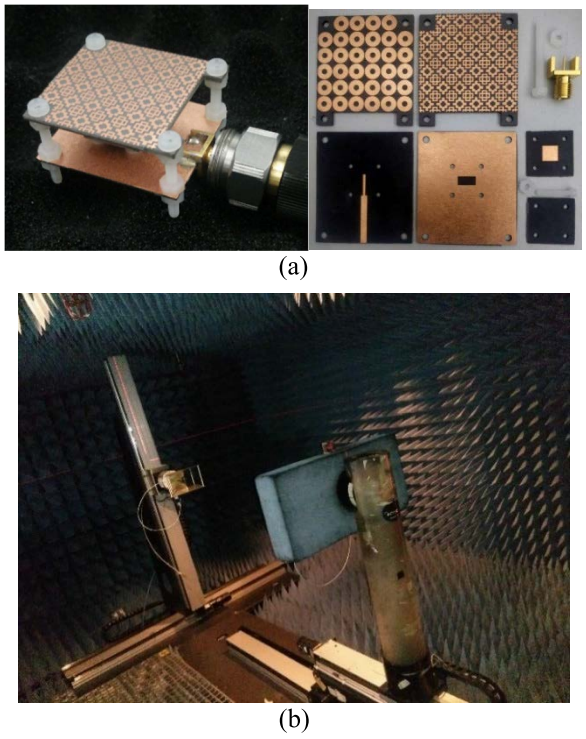

FIGURE 14. Final (a) fabricated antenna and its assembly parts, and (b) far-field measurement setup.

Next, the reflection coefficients characteristics of the fabricated prototype are analyzed and measured using the Agilent 8722ES Vector Network Analyzer, and the results are illustrated in Fig. 15(a), where the measured impedance bandwidth with S_{11} <-10 dB criterion is 6.03 GHz for a wideband FPRA ranging from 11.32 to 17.35 GHz, corresponding to a fractional impedance bandwidth of 42% for the center frequency of interest. It is also compared to the simulated results, where the impedance bandwidth was 38.64 % (5.7 GHz) ranging from 11.9 to 17.6 GHz.

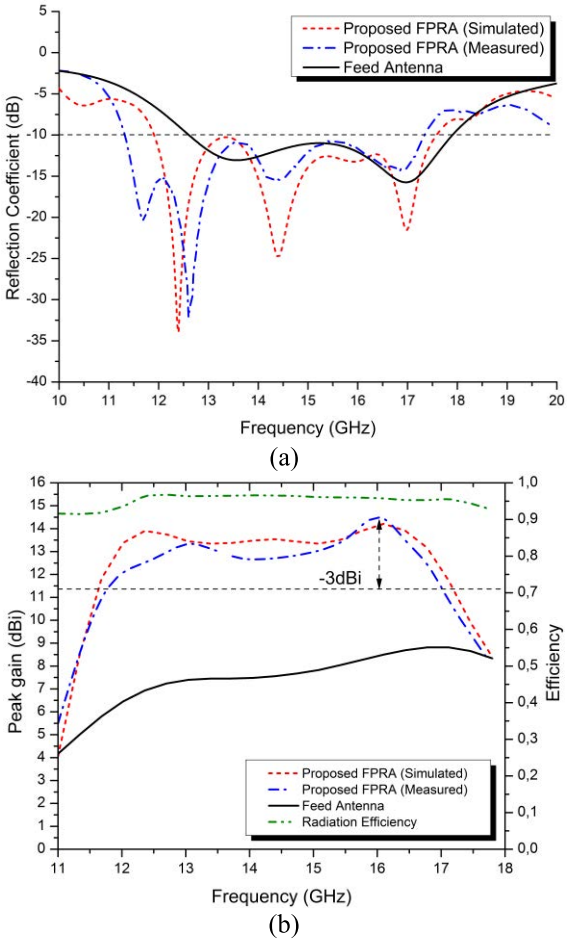

FIGURE 15. (a) Reflection coefficients of the FPRA and (b) gain of the FPRA.

Therefore, both simulation and measurement results are in good agreement, despite the slight discrepancies between them, which are probably due to assembly and fabrication errors. Thus, the proposed antenna performed outstandingly

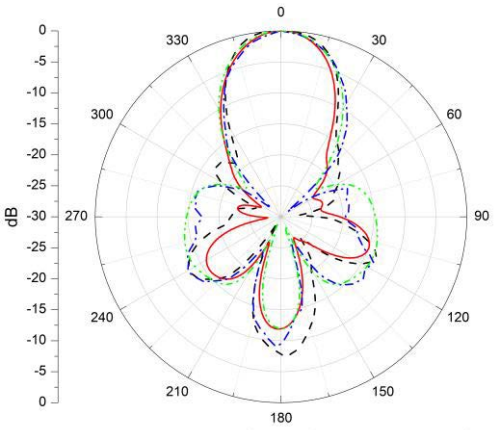

(a)

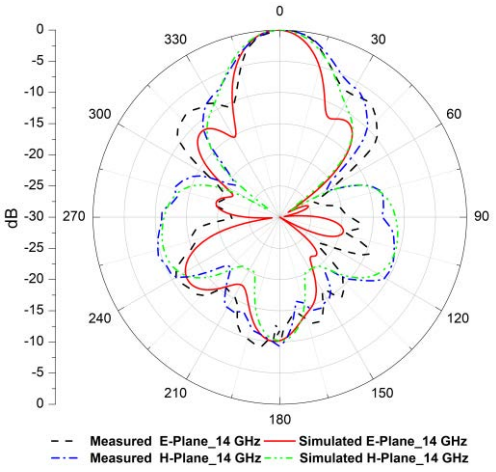

(b)

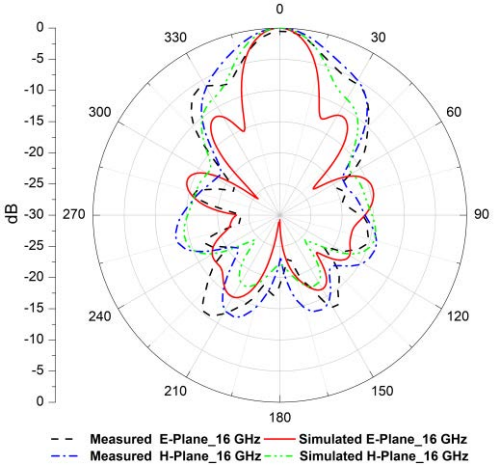

(c)

FIGURE 16. Normalized simulated and measured radiation patterns in the E- and H-planes at (a) 12.5, (b) 14, and (c) 16 GHz.

in terms of wide impedance bandwidth, covering almost the whole Ku-band spectrum.

In addition, the peak gain and radiation patterns for the proposed prototype were measured in an anechoic chamber, and the setup is depicted in Fig. 14(b), by using the following

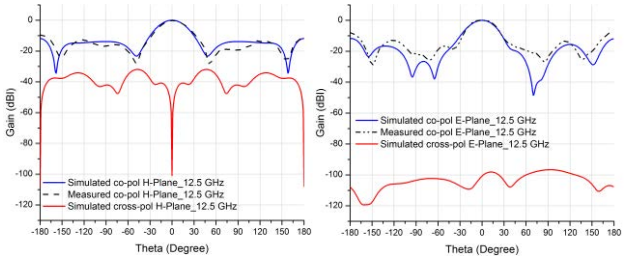

(a)

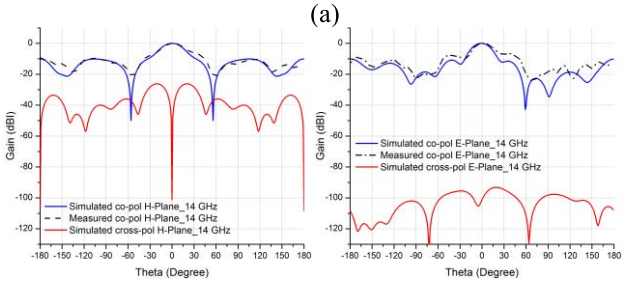

(b)

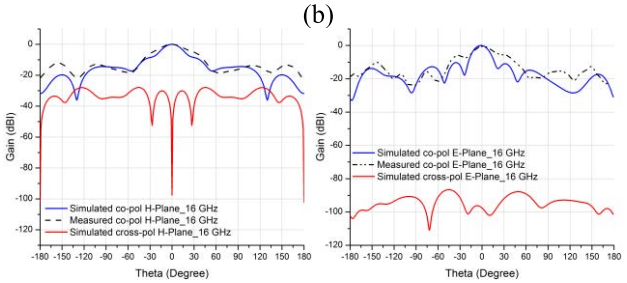

(c)

FIGURE 17. Normalized simulated and measured radiation patterns (Co- & cross-polarization) in the E- and H-planes at (a) 12.5, (b) 14, and (c) 16 GHz.

equation, the gain of the antenna under test (AUT) is calculated [39]:

$$G_{AUT} = G_{horn} - P_{horn} + P_{AUT} \tag{10}$$

where G_{horn} is the gain of the standard horn antenna. P_{horn} and P_{AUT} are the received power of the horn antenna (receiver mode), and the antenna under testing, respectively. The results are depicted in Fig. 15(b), confirming that by using a PRS-based superstrate with a positively gradient phase, the peak gain over a wideband of a frequency spectrum is improved drastically.

From Fig. 15 (b), the measured maximum peak gain of the proposed FPRA is 14.72 dBi at 16 GHz, with a 3-dB gain bandwidth of 36% (5.1 GHz) ranging from 11.68 to 16.78 GHz, which is in good agreement with the simulation results.

For further analysis, the normalized simulated and measured radiation patterns of the proposed FP resonator antenna are illustrated in Fig. 16 & 17 at three different frequencies, 12.5, 14, and 16 GHz, in both H- and E-planes.

The obtained radiation patterns (simulated and measured) of the antenna, are directional in the broadside of both the E- and H-planes, with lower side-lobe and cross-polarization levels, and a narrower beam-width. Both simulation and

measurement results are in good agreement, with a slight difference due to fabrication errors. With these features, the proposed design could be a potential candidate, allowing a high and consistent gain over a larger operating bandwidth, and low profile, for applications in the Ku-band spectrum.

Finally, the proposed FPRA design is compared to others in the literature, taking into account the bandwidth, the maximum peak gain, the overall size of the design, and the number of PRS layers. The comparison is summarized in Table 3. From this comparison, it can be concluded that the proposed design outperforms the other ones in terms of compactness, high gain, and wider operation bandwidth.

IV. CONCLUSION

In this paper, a topology optimized partially reflective surface (PRS) using the genetic algorithm embedded in Matlab, with a VBA-based interface established with CST Microwave studio, has been designed and simulated. This proposed PRS design has provided a positive reflection coefficient phase, which leads to a wider impedance, 3-dB gain bandwidth, and high gain at the Ku band.

The proposed prototype has been fabricated and measured. The simulation results have been validated by measurements, and they have shown a wide −10dB impedance bandwidth of 6.03 GHz ranging from 11.32 to 17.35 GHz, which corresponds to a fractional impedance bandwidth of 42% for the center frequency of interest. In addition, the measured 3-dB gain bandwidth is 5.1 GHz (35.83%) ranging from 11.68 to 16.78 GHz, with a measured peak gain of 14.72 dBi, which is almost double the source antenna's gain.

Aside from the aforementioned improvements, using the proposed PRS layer shaped the radiation pattern to become more directive, with a narrower beam-width and lower side-lobe levels. The simulation and measurement results are in good agreement, with a slight difference due to fabrication errors. The proposed PRS-based FP resonator antenna can be a good candidate for high gain with wideband applications in the Ku-band.

REFERENCES

[1] F. Meng and S. K. Sharma, "A wideband resonant cavity antenna with compact partially reflective surface," *IEEE Trans. Antennas Propag.*, vol. 68, no. 2, pp. 1155–1160, Oct. 2019.
[2] M. Mahajan, R. Jyoti, K. Sood, and S. B. Sharma, "A method of generating simultaneous contoured and pencil beams from single shaped reflector antenna," *IEEE Trans. Antennas Propag.*, vol. 61, no. 10, pp. 5297–5301, Oct. 2013.
[3] H. Deguchi, M. Tsuji, and H. Shigesawa, "Compact low-cross-polarization horn antennas with serpentine-shaped taper," *IEEE Trans. Antennas Propag.*, vol. 52, no. 10, pp. 2510–2516, Oct. 2004.
[4] Y. J. Cheng, Y. X. Guo, and Z. G. Lin, "W-band large-scale high-gain planar integrated antenna array," *IEEE Trans. Antennas Propag.*, vol. 62, no. 6, pp. 3370–3373, Jun. 2014.
[5] S. Jia, Y. B. Li, L. Zhang, Z. J. Luo, B. W. Han, R. Q. Li, X. Y. Cao, Q. Cheng, and T. J. Cui, "Programmable controls to scattering properties of a radiation array," *Laser Photon. Rev.*, vol. 15, no. 2, 2021, Art. no. 2000449.
[6] S. Jia, Y. B. Li, H. Li, Z. X. Wang, C. Zhang, Z. X. Guo, R. Q. Li, X. Y. Cao, Q. Cheng, and T. J. Cui, "A thin self-feeding Janus metasurface for manipulating incident waves and emitting radiation waves simultaneously," *Annalen der Physik*, vol. 532, no. 5, 2020, Art. no. 2000020.
[7] B. Han, S. Li, Z. Li, G. Huang, J. Tian, and X. Cao, "Asymmetric transmission for dual-circularly and linearly polarized waves based on a chiral metasurface," *Opt. Exp.*, vol. 29, no. 13, pp. 19643–19654, Jun. 2021.
[8] Z. Yue, S. J. Li, B. W. Han, G. S. Huang, Z. X. Guo, and X. Y. Cao, "Quad-band transmissive metasurface with linear to dual-circular polarization conversion simultaneously," *Adv. Theory Simul.*, vol. 4, no. 8, 2021, Art. no. 2100117.
[9] S. Li, Z. Li, B. Han, G. Huang, X. Liu, H. Yang, and X. Cao, "Multifunctional coding metasurface with left and right circularly polarized and multiple beams," *Frontiers Mater.*, vol. 9, Feb. 2022, Art. no. 854062.
[10] A. Hosseini, F. D. Flaviis, and F. Capolino, "A 60 GHz simple-to-fabricate single-layer planar Fabry–Pérot cavity antenna," *IET Microw., Antennas Propag.*, vol. 9, no. 4, pp. 313–318, 2015.
[11] H. Attia, M. L. Abdelghani, and T. A. Denidni, "Wideband and high-gain millimeter-wave antenna based on FSS Fabry–Pérot cavity," *IEEE Trans. Antennas Propag.*, vol. 65, no. 10, pp. 5589–5594, Oct. 2017.
[12] N. Wang, Q. Liu, C. Wu, L. Talbi, Q. Zeng, and J. Xu, "Wideband Fabry–Pérot resonator antenna with two complementary FSS layers," *IEEE Trans. Antennas Propag.*, vol. 62, no. 5, pp. 2463–2471, May 2014.
[13] H. H. Tran and T. K. Nguyen, "K-band planar and low-profile Fabry–Pérot cavity antenna with a coupled strip-slitline feed structure," *Appl. Comput. Electromag. Soc. J.*, vol. 32, no. 6, pp. 542–547, Jun. 2017.
[14] Z. G. Liu, Z. X. Cao, and L. N. Wu, "Compact low profile circularly polarized Fabry–Pérot resonator antenna fed by linearly polarized microstrip patch," *IEEE IEEE Antennas Wireless Propag. Lett.*, vol. 15, pp. 524–527, 2015.
[15] Y. F. Cheng, W. Shao, X. Ding, and M. X. Yu, "Design of tilted-beam Fabry–Pérot antenna with aperiodic partially reflective surface," *Appl. Comput. Electromag. Soc. J.*, vol. 32, no. 5, pp. 397–404, May 2017.
[16] Y. Ge, K. P. Esselle, and T. S. Bird, "The use of simple thin partially reflective surfaces with positive reflection phase gradients to design wideband, low-profile EBG resonator antennas," *IEEE Trans. Antennas Propag.*, vol. 60, no. 2, pp. 743–750, Feb. 2012.
[17] M. L. Abdelghani, H. Attia, and T. A. Denidni, "Dual- and wideband Fabry–Pérot resonator antenna for WLAN applications," *IEEE Antennas Wireless Propag. Lett.*, vol. 62, pp. 473–476, 2016.
[18] C. Mateo-Segura, A. P. Feresidis, and G. Goussetis, "Bandwidth enhancement of 2-D leaky-wave antennas with double-layer periodic surfaces," *IEEE Trans. Antennas Propag.*, vol. 62, no. 2, pp. 586–593, Feb. 2014.
[19] N. Z. Wang, J. D. Xu, and Q. S. Zeng, "Broadband EBG resonator antenna using a combination of different dielectric substrates," *IEEE Antennas Propag. Soc. Int. Symp.* Orlando, FL, USA, Jul. 2013, pp. 894–895.
[20] R. M. Hashmi and K. P. Esselle, "A class of extremely wideband resonant cavity antennas with large directivity-bandwidth products," *IEEE Trans. Antennas Propag.*, vol. 64, no. 2, pp. 830–835, Feb. 2016.
[21] R. M. Hashmi, K. P. Esselle, and S. G. Hay, "Directive beaming with lens-like superstates for low profile Fabry–Pérot cavity antennas," in *Proc. 16th Int. Symp. Antenna Tech. Appl. Electromagn.* Victoria, BC, Canada, Jul. 2014, pp. 1–2.
[22] Y. F. Lu and Y. C. Lin, "Design and implementation of broadband partially reflective surface antenna," in *Proc. IEEE Int. Symp. Antennas Propag.* Spokane, WA, USA, Jul. 2011, pp. 2250–2253.
[23] K. Kanjanasit and C. H. Wang, "A broadband resonant cavity antenna using a metamaterial based on double-side identical arrays," in *Proc. IEEE Conf. Antenna Meas. Appl.*, Tsukuba, Japan, Dec. 2017, pp. 51–54.
[24] R. N. Lian, Z. Y. Tang, and Y. Z. Yin, "Design of a broadband polarization-reconfigurable Fabry–Pérot resonator antenna," *IEEE Antennas Wireless Propag. Lett.*, vol. 17, no. 1, pp. 122–125, Jan. 2018.
[25] M. Temmar, A. Hocini, D. Khedrouche, and M. Zamani, "Analysis and design of a terahertz microstrip antenna based on a synthesized photonic bandgap substrate using BPSO," *J. Comput. Electron.*, vol. 18, no. 1, pp. 231–240, Jan. 2019.
[26] Q. Chen, X. Chen, and K. Xu, "3-D printed Fabry–Pérot resonator antenna with paraboloid-shape superstrate for wide gain bandwidth," *Appl. Sci.*, vol. 7, no. 11, p. 1134, 2017.
[27] A. P. Feresidis, G. Goussetis, S. Wang, and J. C. Vardaxoglou, "Artificial magnetic conductor surfaces and their application to low-profile high-gain planar antennas," *IEEE Trans. Antennas Propag.*, vol. 53, no. 1, pp. 209–215, Jan. 2005.
[28] G. Von Trentini, "Partially reflecting sheet arrays," *IRE Trans. Antennas Propag.*, vol. 4, no. 4, pp. 666–671, Oct. 1956.
[29] L. Leger, C. Serier, R. Chantalat, M. Thevenot, T. Monediere, and B. Jecko, "1D dielectric electromagnetic band gap (EBG) resonator antenna design," *Ann. Télécommun.*, vol. 59, nos. 3–4, pp. 242–260, 2004.

[30] F. Meng and S. K. Sharma, "A dual-band high-gain resonant cavity antenna with a single layer superstrate," *IEEE Trans. Antennas Propag.*, vol. 63, no. 5, pp. 2320–2325, May 2015.
[31] N. Melouki, A. Hocini, and T. A. Denidni, "Performance enhancement of a compact patch antenna using an optimized EBG structure," *Chin. J. Phys.*, vol. 69, pp. 219–229, Feb. 2021.
[32] A. Hocini, N. Melouki, and T. A. Denidni, "Modeling and simulation of an antenna with optimized AMC reflecting layer for gain and front-to-back ratio enhancement for 5G applications," *J. Phys., Conf. Ser.*, vol. 1492, no. 1, Apr. 2020, Art. no. 012006.
[33] N. Melouki, A. Hocini, and T. A. Denidni, "Performance enhancement of an ultra-wideband antenna using a compact topology optimized single frequency selective surface-layer as a reflector," *Int. J. RF Microw. Comput., Aided Eng.*, vol. 32, no. 5, 2022, Art. no. e23097.
[34] L. Moustafa and B. Jecko, "Design and realization of a wide-band EBG antenna based on FSS and operating in the Ku-band," *Int. J. Antennas Propag.*, vol. 2010, Mar. 2010, Art. no. 139069.
[35] A. P. Feresidis and J. C. Vardaxoglou, "A broadband high-gain resonant cavity antenna with single feed," in *Proc. EuCA*. Nice, France, Nov. 2006, p. 15.
[36] M. A. Meriche, H. Attia, A. Messai, S. S. I. Mitu, and T. A. Denidni, "Directive wideband cavity antenna with single-layer meta-superstrate," *IEEE Antennas Wireless Propag. Lett.*, vol. 18, no. 9, pp. 1771–1774, Sep. 2019.
[37] R. Garg, P. Bhartia, I. Bahl, and A. Ittipiboon, *Microstrip Antenna Design Handbook*. Norwood, MA, USA: Artech House, 2001, ch. 1, pp. 43–47.
[38] C. Balanis, *Antenna Theory: Analysis and Design*. Hoboken, NJ, USA: Wiley, 2015.
[39] H. Zhu, X. Li, Z. Qi, and J. Xiao, "A 320 GHz octagonal shorted annular ring on-chip antenna array," *IEEE Access*, vol. 8, pp. 84282–84289, 2020.
[40] K. Konstantinidis, A. P. Feresidis, and P. S. Hall, "Broadband subwavelength profile high-gain antennas based on multi-layer metasurfaces," *IEEE Trans. Antennas Propag.*, vol. 63, no. 1, pp. 423–427, Jan. 2015.
[41] N. Wang, J. Li, G. Wei, L. Talbi, Q. Zeng, and J. Xu, "Wideband Fabry–Pérot resonator antenna with two layers of dielectric superstrates," *IEEE IEEE Antennas Wireless Propag. Lett.*, vol. 14, pp. 229–232, 2015.
[42] K. Konstantinidis, K. P. Feresidis, and P. S. Hall, "Multilayer partially reflective surfaces for broadband Fabry–Pérot cavity antennas," *IEEE Trans. Antennas Propag.*, vol. 62, no. 7, pp. 3474–3481, Jul. 2014.
[43] N. Wang, L. Talbi, Q. Zeng, and J. Xu, "Wideband Fabry–Pérot resonator antenna with electrically thin dielectric superstrates," *IEEE Accesss*, vol. 6, pp. 14966–14973, 2018.

NOUREDDINE MELOUKI received the B.Sc., M.Sc., and Ph.D. degrees in telecommunication engineering from the University of M'Sila, Algeria, in 2012, 2014, and 2021 respectively. He is currently pursuing the second Ph.D. degree with the Institut National de la Recherche Scientifique (INRS), Université du Quebec, Montreal, QC, Canada.

His main field of research includes microwave/millimeter-wave, metamaterials including EBG/PBG, AMC, and FSS/PRS structures. In addition to reconfigurable antennas, array antennas, MIMO antennas, as well as RF/microwave components for wireless communications systems. His current research interests include high-gain and miniaturized antennas for the future wireless communication systems, namely 5G.

ABDESSELAM HOCINI received the Engineer, Magister, and Ph.D. degrees in electronics instrumentation from Constantine University, Algeria, in 2000, 2002, and 2008, respectively.

He is currently a Professor with the Electronics Department and also the Head of the Signals and Systems Analysis Laboratory, Mohamed Boudiaf University of M'sila, Algeria. His research interests include the design and characterization of photonic devices. In particular, his research concerns sensor, plasmonic, and realizing advanced functional photonic crystal devices, in addition to his expertise in antenna and communication systems design including metamaterial such as EBG/PBG, FSS, and AMC, in both microwave and millimeter spectrums.

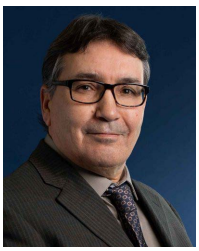

TAYEB A. DENIDNI (Fellow, IEEE) received the M.Sc. and Ph.D. degrees in electrical engineering from Laval University, Quebec, QC, Canada, in 1990 and 1994, respectively.

He was a Professor at the Engineering Department, Université du Quebec in Rimouski, Rimouski, QC, Canada, from 1994 to 2000, where he founded the Telecommunications Laboratory. Since 2000, he has been with the Institut National de la Recherche Scientifique (INRS), Université du Quebec, Montreal, QC, Canada. He founded the RF Laboratory with INRS-EM, Montreal. He has extensive experience in antenna design and leading a Large Research Group consisting of three research scientists, eight Ph.D. students, and two M.Sc. students. His current research interests include reconfigurable antennas using EBG and FSS structures, dielectric resonator antennas, metamaterial antennas, adaptive arrays, switched multi-beam antenna arrays, ultra-wideband antennas, microwave, and development for wireless communications systems. From 2005 to 2007, he served as an Associate Editor for the IEEE Antennas and Wireless Propagation Letters. He served as an Associate Editor for the IEEE Transactions on Antennas and Propagation, from 2008 to 2010. Since 2015, he has been served as an Associate Editor for *IET Electronics Letters*.